RUSSIAN JOURNAL of EARTH SCIENCES Online ISSN: 1681-1208

SPECIAL ISSUE: "KAMCHATKA EARTHQUAKE M 8.8 ON JULY 29, 2025"

RESPONSE OF GEOFLUID SYSTEMS TO THE ACTIVATION OF REGIONAL SEISMICITY IN KAMCHATKA IN JULY 2025

A. V. Solomatin[1], A. V. Kiryukhin[1,2,*], A. Yu. Polyakov[1], M. V. Lemzikov[1], D. N. Burnaikin[3], V. P. Petrochenko[4], G. N. Kopylova[5], G. V. Ryabinin[5], Yu. V. Demyanchuk[1,5], and O. O. Usacheva[1]

[1]Institute of Volcanology and Seismology FEB RAS, Petropavlovsk-Kamchatsky, Russian Federation
[2]Kronotsky Federal Nature Biosphere Reserve, Elizovo, Russian Federation
[3]"Teplo Zemli" JSC, Termalny, Kamchatka Krai, Russian Federation
[4]"Bystrinskaya Gornaya Compania" JSC, Petropavlovsk-Kamchatsky, Russian Federation
[5]Kamchatka Branch of the Geophysical Survey of the Russian Academy of Sciences, Petropavlovsk-Kamchatsky, Russian Federation
* **Correspondence to:** Alexey Kiryukhin, AVKiryukhin2@mail.ru

Abstract: Geofluid systems are unique geomechanical sensors, as they can generate earthquakes themselves and also respond to changes in Earth activity. The $M_W = 8.8$ earthquake of July 29, 2025 in Kamchatka was accompanied by numerous geofluid anomalous phenomena: (1) regional seismogenic faults activity; (2) significant post-seismic decreases in water levels (the first meters) and rates in wells of low temperature geothermal fields (Vilyuchinsky, Paratunsky and Ketkinsky); (3) omissions of eruptions of the Bolshoy geyser (Valley of Geysers) and the emergence of a new geyser-well (Kumroch); (4) the beginning of volcanic eruptions (Krasheninnikov volcano for the first time in ~600 years, Klyuchevskoy volcano) and volcanoes activity increase (Karymsky, Mutnovsky, Kambalny). In this study, the ability of geofluid systems to track seismic events was used to identify the activity of regional seismogenic faults and volcanic magmatic systems (the Frac-Digger method). This provides an explanation for the observed phenomena in terms of the geomechanical regional stretching of Kamchatka, which was associated with an $M_W = 8.8$ earthquake followed by a decrease in geofluid pressure. In magma systems of volcanoes, this triggered boiling and gas-lift of magma with subsequent eruptions. In the fractured-type reservoirs of low-temperature hydrothermal systems, this led to a significant drop in water levels and a cessation of discharge. In the high-temperature and gas-rich Valley of the Geysers Field, this led to the disintegration of the caprock and the infiltration of water, resulting in the subsequent eruptions of the Grotto and the Great Geyser being skipped, while the Kumroch CO_2 reached the hydrothermal reservoir, boiled, and began cycling eruptions. These phenomena are consistent with the models of the $M_W = 8.8$ earthquake's focal mechanism and satellite geodetic data from GNSS and InSAR.

Keywords: Frac-Digger, fluid pressure, geomechanics, magma boiling, CO_2 gas-lift, regional extension, geysers, water level, drop, eruptions, volcanoes, faults, Kamchatka megathrust earthquake

Citation: Solomatin A. V., Kiryukhin A. V., Polyakov A. Yu., Lemzikov M. V., Burnaikin D. N., Petrochenko V. P., Kopylova G. N., Ryabinin G. V., Demyanchuk Yu. V., and Usacheva O. O. (2026), Response of Geofluid Systems to the Activation of Regional Seismicity in Kamchatka in July 2025, *Russian Journal of Earth Sciences*, 26, ES2014, EDN: ORNLAF, https://doi.org/10.2205/2026es001124

RESEARCH ARTICLE

Received: February 2, 2026
Accepted: May 25, 2026
Published: July 1, 2026

1. Introduction

Geofluid systems are unique geomechanical sensors, as they can generate earthquakes themselves and also respond to changes in geomechanical activity.

The system of regional seismogenic faults [*Avdeiko and Palueva*, 2010, 2011, 2012; *Seliverstov*, 2007; *Zavaritsky*, 1955], determined by seismotectonic [*Lobkovsky and Baranov*, 1984; *Zelenin et al.*, 2022] and geofluid [*McClure*, 2012] processes of various hierarchical levels, was detected here in the form of plane-oriented clusters of hypocenters of regional earthquakes. These clusters may include events defined by S. A. Fedotov as the "strongest earthquakes" for the Kuril-Kamchatka region [*Fedotov*, 2005]. Specifically, those with a magnitude of $M \geq 7.7$, as the development of the foci of these particular events exerts a primary control on the regional seismic process.

Volcanic magmatic activity, which takes the form magma fracking [*Kiryukhin et al.*, 2022b] with the injection of dykes and sills, was detected as plane-oriented clusters of microearthquake (MEQ) hypocenters [*Kiryukhin et al.*, 2016; *Sigmundsson et al.*, 2015]. Regional catalogs of seismic events are used to identify the orientation and dynamics of regional seismogenic faults, while local catalogs of seismic events are used to identify the orientation and dynamics of magmatic injections under volcanoes. The data is processed using the Frac-Digger program [*Kiryukhin et al.*, 2016].

Monitoring of pressure in hydrothermal and hydrogeological reservoirs is carried out as part of standard hydrogeological observations by companies operating geothermal fields (JSC Teplo Zemli, PJSC Kamchatskenergo). Observations of geyser activity (interval between eruptions) are carried out using autonomous temperature loggers [*Kiryukhin*, 2016].

The assumption of the frictional equilibrium of seismogenic faults [*Zoback*, 2010], experience of applying the geomechanical principles of hydraulic fracturing to describe the formation of dyke fields [*Andrew and Gudmundsson*, 2008; *Gudmundsson*, 2006, 2011, 2020, 2022; *Gudmundsson and Andrew*, 2007] and hydrogeological indicators of seismic activity [*Björnsson et al.*, 2001; *Kissin*, 2009] are used to analyze the functioning of regional seismogenic faults, hydrogeodynamic perturbations in hydrothermal reservoirs and magma systems of volcanoes [*Fedotov*, 2006; *Gordeev et al.*, 2020a,b].

Precise observations of pressure variations with a frequency of 1 Hz, temperature, and electrical conductivity of underground water are conducted by the Kamchatka Branch of the Geophysical Survey of the Russian Academy of Sciences (KB GS RAS) in four deep (600–800 m) wells in the Petropavlovsk-Yelizovo urban agglomeration. A description of the observation wells, the equipment used, as well as the seismic and hydrogeological effects recorded during the strong Kamchatka earthquakes in 1997–2023 is given in the works [*Boldina et al.*, 2022; *Kopylova and Boldina*, 2023, 2025]. The method of assessing the volumetric co-seismic strain of water-bearing rocks based on precision observations in piezometric wells is presented in the work [*Kopylova and Boldina*, 2023].

Thus, this paper examines the response of geofluid systems above mentioned (hydrothermal and hydrogeological reservoirs, magmatic feeding systems of volcanoes, and regional seismogenic faults) to the $M_W = 8.8$ earthquake that occurred in Kamchatka on July 29, 2025.

2. Materials and Methods

2.1. Activation of Seismogenic Faults

The study used two databases for the period January 1, 1980–January 10, 2026: from the regional earthquake catalog of the KB GS RAS [*Chebrov et al.*, 2013] and the global catalog of NEIC USGS. The first of these databases includes 16,249 events with a class K_s of at least 9.5, and the second includes 6,584 events with a magnitude M (mb) of at least 4.2. The use of two catalogs instead of one is due to their fundamental drawbacks: possible systematic errors in determining the epicenters of earthquakes based on the near-linear configuration of the regional network, and significant errors in determining the depths of these events when they are recorded by significantly distant seismic stations in the global network.

The identification of plane-oriented clusters of earthquake hypocenters in the above-mentioned area was carried out using the following control parameters of the Frac-Digger program: (1) the number of events per selected cluster is $N \geq 30$; (2) the time period determining the samples for cluster construction is unlimited (discontinuous structures in the earthquake source area are formed at least during the III stage of the seismic cycle for about 15–20 years); (3) the permissible deviation of the event from the cluster plane is $\delta Z \leq 5$ km; (4) the permissible maximum size of the selected cluster in the horizontal plane is $\delta R \leq 100$ km.

Calculations based on these parameters using the regional earthquake catalog made it possible to identify 133, and based on the NEIC catalog – 75 seismogenic faults (Figure 1). Of the 133 seismogenic faults identified during the specified period, 87 showed signs of activation (added by earthquake hypocenters) after the $M_W = 8.8$ earthquake). Of these 87 faults, 24 showed signs of the greatest aftershock activity (more than 30 hypocenters were added) – all of them belong to the area of the focus of the specified mega-earthquake and its immediate surroundings, 38 more faults showed moderate aftershock activity (from 5 to 27 hypocenters were added), the remaining 25 had weak aftershock activity (from 0 to 4 hypocenters were added).

Statistical analysis of the geometric parameters of seismogenic faults (angle and dip azimuth, strike azimuth, and depth of the center) shows the following: (1) seismogenic faults with the highest aftershock activity (Figure 1, highlighted in yellow, and Figure 2) are characterized by a clear predominance of dip azimuths of 285–330° and 120–135° (strike northeast, north-northeast), and dip angles of 20–30° and 40–50° (predominant), with a depth of the centers below 70 km; (2) seismogenic faults with no aftershock activity are characterized by a dominance of dip azimuths of 240–300° (submeridional strike), and dip angles of 50–60°.

A comparison of the total number of seismogenic faults and seismogenic faults with the highest aftershock activity shows that the direction of the maximum horizontal stress $S_{H\max}$ after $M_W = 8.8$ on July 29, 2025 has rotated clockwise by 10° (Figure 2).

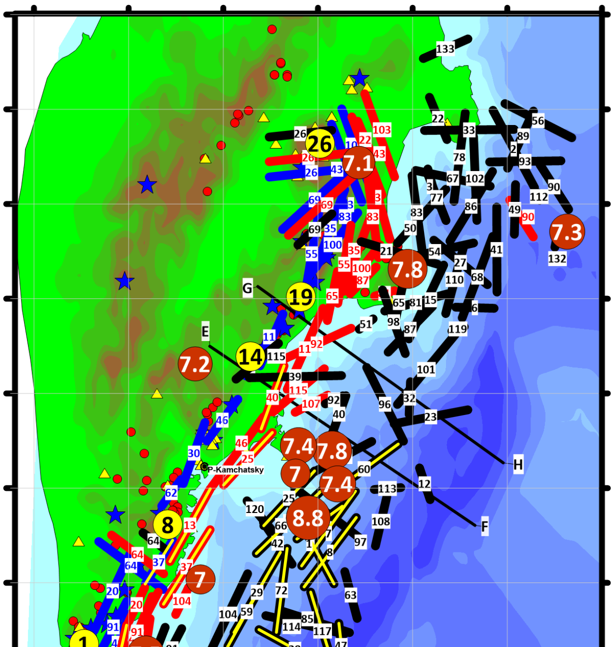

Figure 1. Map of seismogenic faults, active volcanoes, and hydrothermal systems. Legend: traces of seismogenic faults based on data from the KB GS RAS (1980–2025) at depths of 20 km, 100 km and 150 km are numbered and colored in black, red and blue lines, respectively, the seismogenic faults with the greatest aftershock activity are highlighted by thin yellow lines from the inside; red circles with numbers inside are the epicenters of an earthquake with magnitudes of at least 7.0 (NEIC); active volcanoes – blue stars; hydrothermal discharges with temperatures from 50 to 100°C – red circles; yellow circles with numbers inside – volcanoes (1 – Kambalny, 8 – Mutnovsky, 14 – Karymsky, 19 – Krasheninnikov, 26 – Klyuchevskoy), activated after the earthquake $M_W = 8.8$ July 29, 2025; yellow triangles – seismic stations of the KB GS RAS. Scale marking – 100 km.

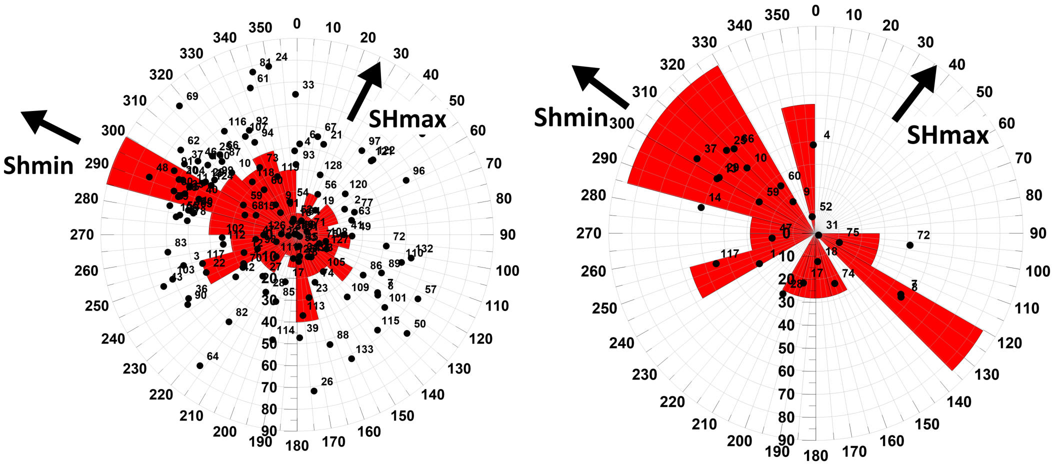

Figure 2. Stereograms (dip angle, dip azimuth) and rose-diagram (dip azimuth) of the regional seismogenic faults (numbered according to Figure 1), detected on data from the KB GS RAS (1980–2025). Left figure shows all seismogenic faults, right figure shows seismogenic faults with the highest aftershock activity after $M_W = 8.8$ July 29, 2025 (shown by yellow in Figure 1). Note, the direction of the maximum horizontal stress $S_{H\,max}$ after $M_W = 8.8$ on July 29, 2025 has rotated clockwise by 10°.

2.2. Abnormal Hydrogeological Phenomena Synchronized with the $M_W = 8.8$ Earthquake on July 29, 2025

At the Ketkinsky geothermal field, a decrease in the wellhead parameters was recorded at the production wells K01 and K6 (the location of the wells is shown in Figure 3, see also [*Kiryukhin et al.*, 2022a] for detailed description of the Ketkinsky geothermal field). At well K6 showed a drop in flow rate to a complete cessation of flow 30 minutes after the end of the $M_W = 8.8$ earthquake on July 29, 2025, and at well K01 from 1.22 l/s at a temperature of 64.0°C to 1.06 l/s at a temperature of up to 62.0°C 7.5 hours after the earthquake. The temperature at this well gradually continued to decrease and at the end of the year was 55.9°C. The working pressure at the wellhead of K01 decreased after the $M_W = 8.8$ earthquake from 1.2 bar to 0.8 bar. By December 2025, it had recovered to 1.1 bar. K6 also responded to the $M_W = 7.8$ earthquake of September 18, 2025, near Cape Shipunsky.

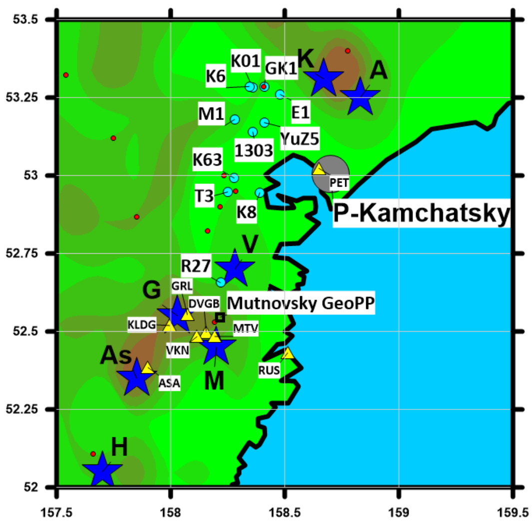

Figure 3. Map of monitoring hydrogeological wells (light blue circles with denotes) and Mutnovsky seismic stations network (yellow triangles with denotes), referenced in this paper. Other legend: blue stars – volcanoes (H – Hodutka, As – Asacha, M – Mutnovsky, G – Gorely, V – Vilyuchinsky, A – Avachinsky, K – Koryaksky), small red circles – hot springs.

The GK1 well was drilled in 1970 to search for thermomineral waters (the location of the well is shown in Figure 3). The well is 1261 m deep. The well is equipped with a head, from which water flows out in a free-flowing mode. Regular observations at the GK1 well are carried out at 6-day intervals.

The hydrogeological effects in the GK1 well mode in connection with the strongest seismic events of 2025 were unique (Figure 4). Previously, the hydrogeological effects of strong earthquakes in the GK1 well mode manifested themselves in the form of an increase in the flow rate and mineralization of the flowing water, as was the case, for example, after the earthquake of August 18, 2024 (Figure 3). A slight increase in the flow rate of the well was also observed after the earthquake of July 20, 2025. After the Kamchatka mega-earthquake on July 29, 2025, and its strongest aftershock on September 19, 2025, the opposite effects were observed, namely a sharp decrease in the well's water flow rate and mineralization. The well's water temperature did not show any significant post-seismic variations, despite seasonal changes. The nature and amplitude of changes in the well's water flow rate and mineralization after the $M_W = 8.8$ Kamchatka earthquake on July 29, 2025, and its strongest aftershock on September 19, 2025, are likely to be explained by the co-seismic deformation of the water-bearing rocks.

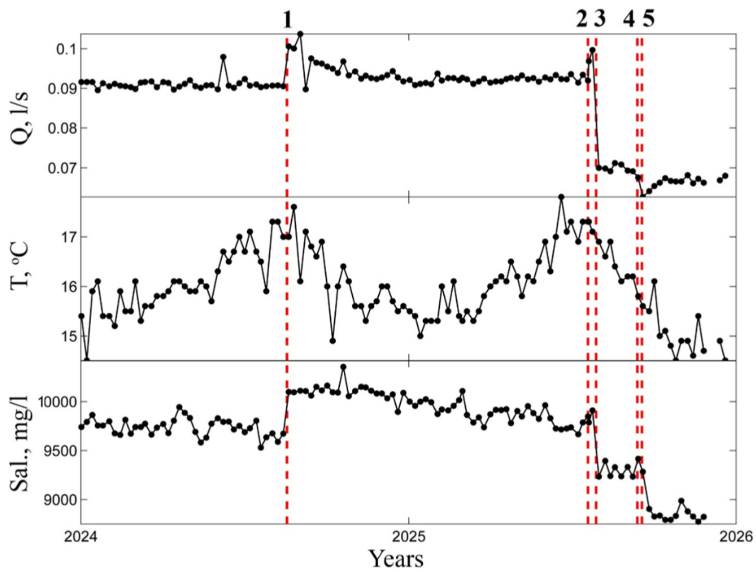

Figure 4. Changes in the flow rate (Q), temperature (T), and water salinity (Sal.) of the self-flowing well GK1 in connection with the strongest earthquakes of 2024–2025. The vertical dotted lines indicate the times of the seismic events on the time axis. The numbers above the vertical dotted lines correspond to earthquakes: 1 – August 18, 2024, $M_W = 7.0$; 2 – July 20, 2025, $M_W = 7.3$; 3 – July 29, 2025, $M_W = 8.8$; 4 – September 13, 2025, $M_W = 7.3$; 5 – September 19, 2025, $M_W = 7.8$.

A decrease in hydrodynamic parameters was also recorded at the Paratunsky geothermal field (information on the field is provided in [*Kiryukhin et al.*, 2017]). At the Sredny Site of well T3, at the Northern Site of well K63, and at well K8 of the Yuzhno-Berezhny Site (the location of the wells is shown in Figure 3), self-flowing stop was detected.

At the Vilyuchinsky R27 well (the location of the well is shown in Figure 3, see also [*Kiryukhin et al.*, 2022b] for detailed field description), the water level was below the wellhead until June 24, 2025, when it began to rise seasonally from mid-May, followed by the spontaneous flow of thermal water from the well. After the $M_W = 8.8$ earthquake, the water flow stopped and the level dropped by 4.5 m, which was immediately after the $M_W = 8.8$ earthquake on July 29, 2025 (Figure 5).

No changes were observed at the Pauzhetsky geothermal field (hydrogeological information about the field is provided in [*Kiryukhin and Yampolsky*, 2004]).

In connection with the $M_W = 8.8$ earthquake, according to precision observations of the KB GS RAS, various seismic-hydrogeodynamic effects were recorded in piezometric

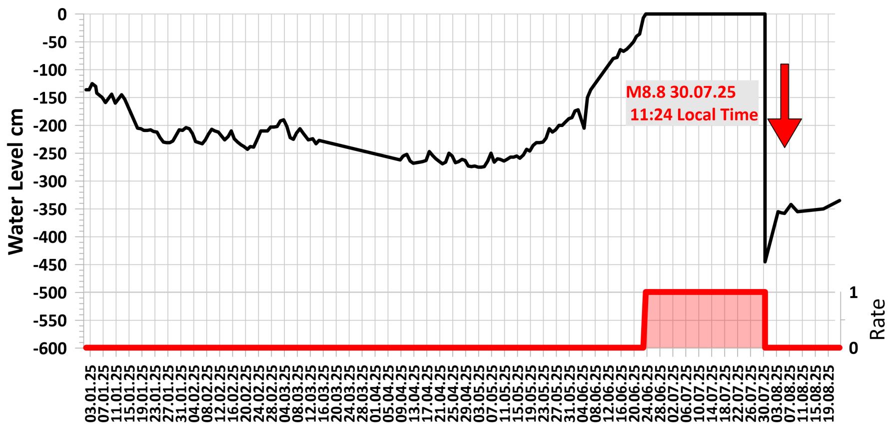

Figure 5. Results of water level monitoring at well R27 (the location of the well is shown in Figure 3) of the Vilyuchinsky geothermal field. Until June 24, 2025, the water level was below the wellhead, then the outflow of thermal water began, which stopped immediately after the $M_W = 8.8$ earthquake on July 29, 2025, and the water level dropped by 4.5 m. Red graph shows flowing conditions: Rate=0 – no flow, Rate=1 – self discharge.

wells (wells YuZ5, 1303, E1 and M1; the location of the wells is shown in Figure 3, see also [*Boldina et al.*, 2022] for details): (1) pressure fluctuations during the passage of seismic body waves with amplitudes of 7–80 hPa in piezometric wells; (2) co-seismic drops in the water pressure in for about one and a half hours after the arrival of seismic waves with amplitudes of −440 hPa (YuZ5, Figure 6) and −580 hPa (1303), corresponding to the value of 2.7×10^{-6} volumetric expansion strain of the water-bearing rocks [*Kopylova and Boldina*, 2023, 2025]; (3) slow recovery of water level/pressure after seismic depressions to their background seasonal values.

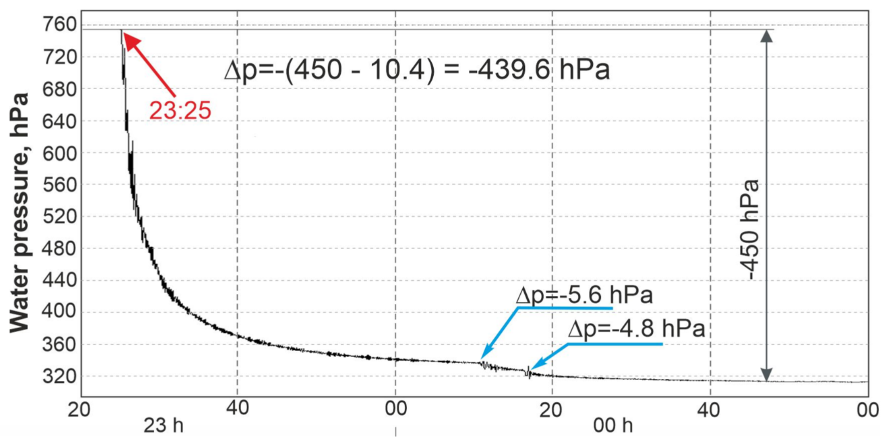

Figure 6. Water pressure drop in well YuZ5 during the time from July 29, 2025, 23:20:00 to July 30, 2025, 01:00:00 and an estimate of the amplitude of the co-seismic pressure drop $\Delta p = -439.6$ hPa due to the $M_W = 8.8$ mega-earthquake (the red arrow indicates the arrival of seismic waves). Blue arrows show co-seismic pressure drops during strong aftershocks on July 30, 00:10 ($M_W = 7.0$, $\Delta p = -5.6$ hPa) and 00:16 ($M_W = 6.8$, $\Delta p = -4.8$ hPa).

In well 1303, the hydrogeodynamic regime was fully restored in October 2025. In well YuZ5, the hydrogeodynamic regime is still being restored: as of January 2026, the water level remains abnormally low by about 2 m compared to its seasonal value.

In well E1, a co-seismic decrease in water level with an amplitude of about 30 cm was recorded for the first time within three weeks after the $M_W = 8.8$ earthquake. Since late September, there has been a gradual recovery of the water level, with an amplitude of up to 10 cm.

In the self-flowing well M1, an $M_W = 8.8$ earthquake caused fluctuations in water pressure in the wellbore during the passage of seismic waves, as well as a co-seismic pressure drop of 0.1 bar over the course of an hour and a half, and an increase in the electrical conductivity and temperature (by 0.5°C) of the underground water. The increased temperature and electrical conductivity of the water have persisted to the present day.

Since 2008, continuous monitoring of the interval between eruptions (IBE) of the Bolshoy, Velikan, Grot, and Shaman (Uzon) geysers has been conducted in the Valley of Geysers and the Uzon Caldera (Figure 7) [*Kiryukhin et al.*, 2022c, 2023b, 2025]. No discrete changes in the IBE (Interval Between Eruptions) of any of the geysers were observed after the $M_W = 8.8$ earthquake on July 29, 2025. Nevertheless, we note the following anomalous features in Figure 7: (1) During the period from May to August 2025, Geyser Bolshoy "missed" at least 12 eruptions, which usually occur every 80 minutes; (2) Geyser Grot stopped its eruptive activity 4–5 months before the $M_W = 8.8$ earthquake.

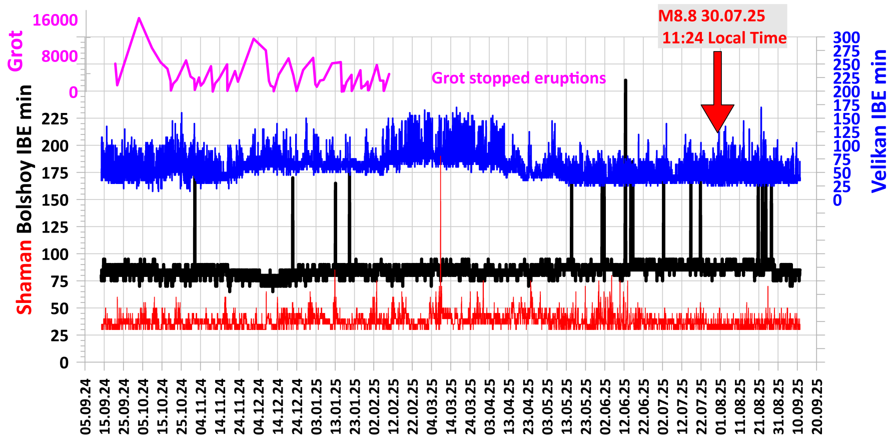

Figure 7. Interval between eruptions (IBE, min) of the Bolshoy, Velikan, Grot, and Shaman (Uzon) geysers on the eve of and after the $M_W = 8.8$ earthquake on July 29, 2025.

In the Kumroch gold ore deposit area, 720 m from the Kruchinsky spring (a carbon dioxide spring with a temperature of 45°C), a well was discovered in September 2025 (Figure 8) that operates in a geyser mode (1 eruption per second, 40°C), although previously (the well was drilled in 2019) it had discharged a small amount of warm water (from a depth of 181 m). The coordinates of the wellhead are (E161.2954°, N55.6996°), the elevation is 563.8 m, the well is not vertical, the angle of inclination is 35° from horizontal, and the true azimuth is 15°.

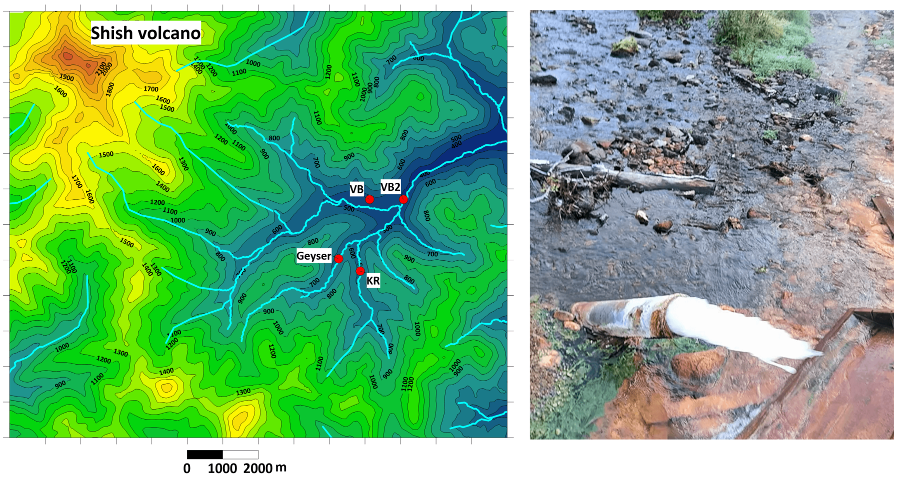

Figure 8. Scheme of testing thermal springs and a geyser-well (photo on the right), discovered in September 2025 at the Kumroch gold ore deposit. Photo by V. P. Petrochenko.

2.3. Volcanic Eruptions and Magmatic Activity Synchronized with the $M_W = 8.8$ Earthquake on July 29, 2025

2.3.1. Mutnovsky Volcano

In 2025, seismic activity at the Mutnovsky Volcano was recorded by eight seismic stations of the KB GS RAS (MTV, GRL, ASA, RUS, PET, DVGB, KLDG, VKN (the location of the seismic stations is shown in Figure 3). After the $M_W = 8.8$ earthquake on July 29, 2025, increased seismic activity was recorded at the Mutnovsky Volcano, and a thermal anomaly was detected using KVERT (Kamchatka Volcanic Eruption Response Team) satellite data.

The Frac-Digger method (sampling criteria ($\delta t = 30$ days, $\delta R = 6$ km, $\delta Z = 1$ km, $N = 6$)) revealed 17 magma injections ($N > 15$) in 2025, Figure 9 shows their projections on the vertical submeridional section of the Mutnovsky geothermal area. Magma injections that occurred after the $M_W = 8.8$ earthquake on July 29, 2025 are highlighted in yellow and labeled in Figure 9. Note the most significant magma injection in the form of dyke #239 ($N = 293$, dip angle 45°, dip azimuth 44°, center depth −1.4 km, $K_{s\max} = 4.3$), which started to inject on August 12, 2025.

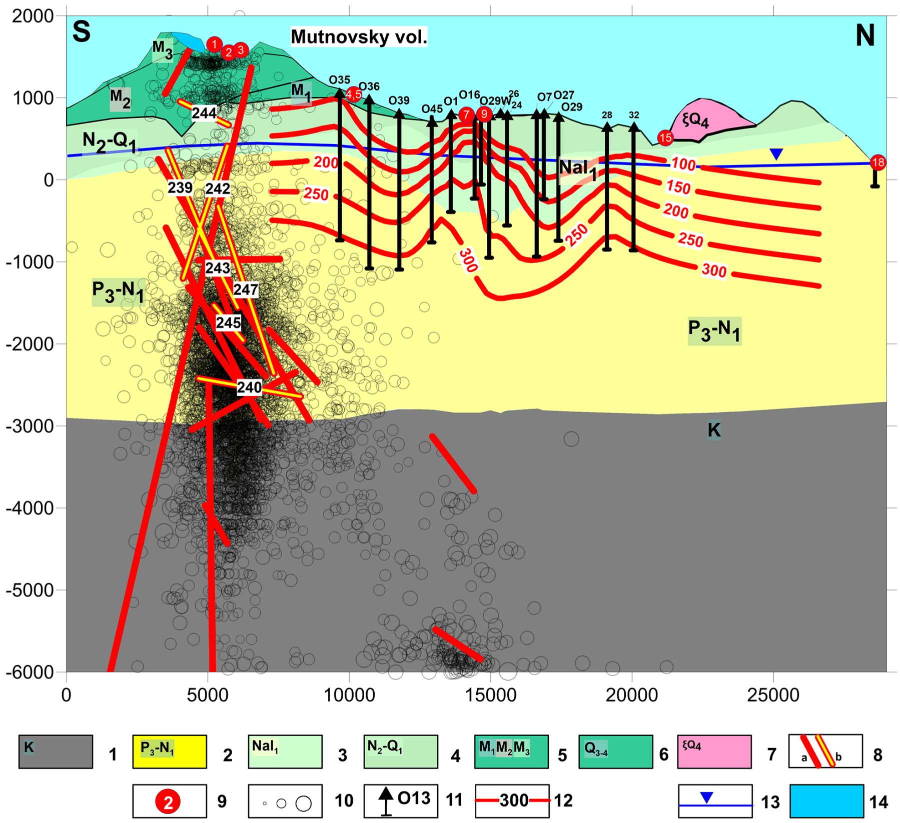

Figure 9. Geological section of the Mutnovsky geothermal area in a submeridional direction. Legend: 1 – Cretaceous basement; 2 – Miocene sandstones and Tertiary volcano-sedimentary deposits; 3 – Miocene dacite and rhyolite tuffs and lavas; 4 – Pliocene-Quaternary basalts and andesite tuffs and lavas; 5 – Mutnovsky 1, 2 and 3 volcanic cones, respectively; 6 – Upper Pleistocene and Holocene andesites and basalts; 7 – Upper Pleistocene and Holocene rhyolite extrusions; 8 – Magmatic injection identified by seismic data from the local network of the KB GS RAS in 2025, with thick red lines, (a), and the same after the $M_W = 8.8$ earthquake on July 29, 2025, with yellow lines and numbers (b); 9 – thermal features (referenced in [*Kiryukhin et al.*, 2022b]); 10 – the hypocenters of earthquakes (2009–2025) within a ±2 km band from the section plane; 11 – wells with corresponding numbers; 12 – isotherms, °C; 13 – geothermal production reservoir water level; and 16 – Mutnovsky volcano glacier. The axes are marked in meters.

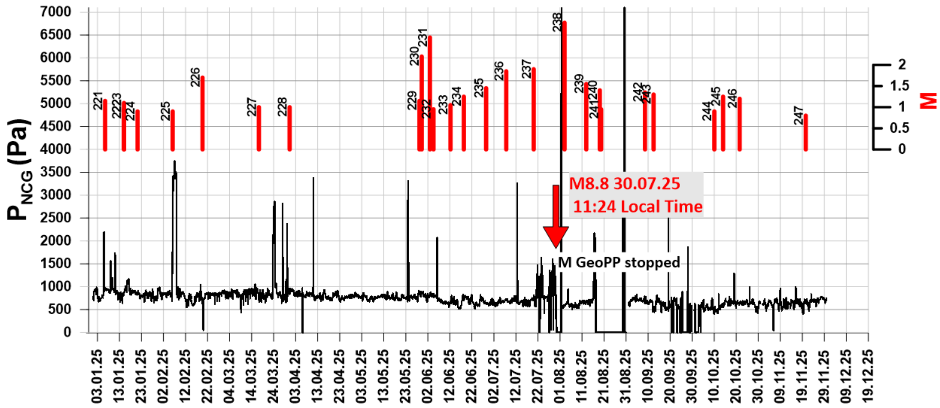

Figure 10. Partial pressure of non-condensable gas P_{NCG} (Pa) in the turbine condenser of the Mutnovsky GeoPower Plant in 2025 and dyke injections (M) from Mutnovsky volcano as a function of time. Dykes numbers corresponds to Figure 9, M correspond to maximum MEQ magnitude, associated with dyke injection.

Aiming estimation of the magmatic gas content, continuous monitoring of the non-condensable gases (most of gas content is CO_2) partial pressure in the turbine condenser of the Mutnovsky geothermal power plant (M GeoPP) performed since 2019 [*Kiryukhin et al.*, 2022b]. To estimate P_{CO_2} (partial CO_2 pressure), using simultaneous measurements of the steam condensate pressure P_c and temperature T_c, yields P_{CO_2} as a difference between P_c and saturation pressure corresponding to temperature T_c.

Figure 10 shows the transient change in P_{CO_2} during the observational period of time from January 1, 2025 to July 29, 2025 (when Mutnovsky GeoPP stopped due to earthquake $M_W = 8.8$). The fluctuations in P_{CO_2} of ±750 Pa during the week before $M_W = 8.8$ on July 29, 2025, as well as the increase in the number of dyke injections between June and August 2025, are clearly visible.

2.3.2. Klyuchevskoy Volcano

The seismic and volcanic activity of Klyuchevskoy volcano was intensified after the $M_W = 8.8$ earthquake of July 29, 2025. "A summit explosive-effusive eruption of the volcano continues. Satellite data by KVERT showed explosions sending ash up to 9–10 km above sea level, and the ash plume is extending for 515 km to the south-east of the volcano. A move of lava flows and ash emission from the summit crater of the volcano continues" (according to KVERT from August 8–12, 2025). Intense fountaining of hot bombs began (Figure 11), with large volumes of pyroclastic material being ejected onto the slopes. The lava flow descended towards the Bogdanovich Glacier. The melting of ice led to the release of huge masses of water, which flowed down the slope. This caused powerful mudflows. On July 30, 2025, a strong ash-fall was observed in the village of Klyuchi in the Ust-Kamchatka District.

Using the Frac-Digger method (sample criteria ($\delta t = 30$ days, $\delta R = 12$ km, $\delta Z = 1$ km, $N = 6$)), 61 magma injections ($N > 30$) were identified in 2025, and their projections on a vertical submeridional section passing through the Klyuchevskoy and Bezymyanny volcanoes are shown in Figure 11. Magma injections that occurred after the $M_W = 8.8$ earthquake on July 29, 2025 are highlighted by yellow lines in Figure 11. The greatest magmatic activity is recorded in the shallow magmatic system of the Klyuchevskoy volcano in the form of sills at about +1 km. We note a significant magma injection in the form of dyke #4072 (highlighted in Figure 11, $N = 149$, dip angle 79°, dip azimuth 34°, center depth +0.8 km, $K_s = 5.3$), injected on August 13, 2025.

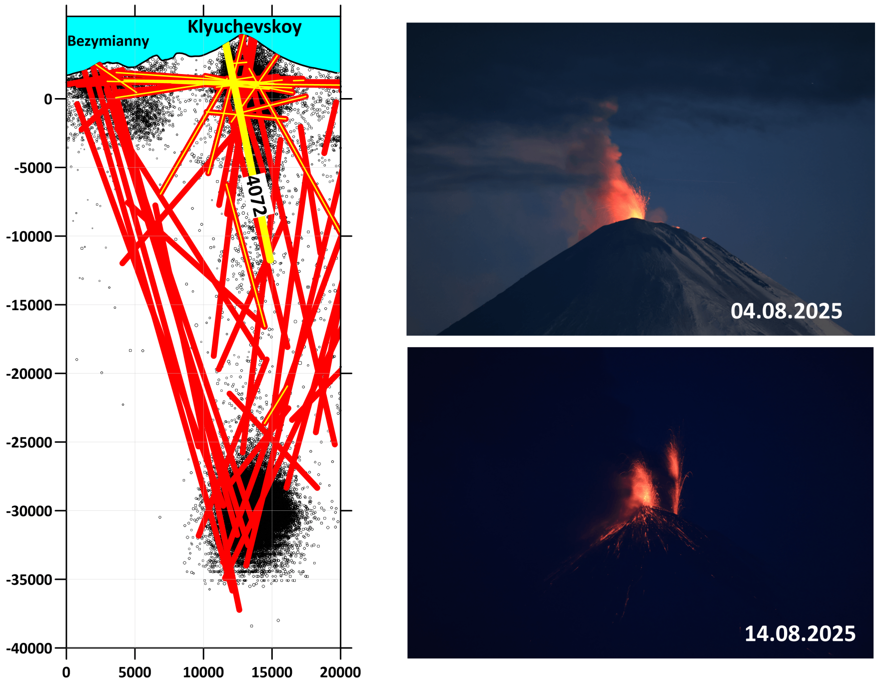

Figure 11. Vertical section through Klyuchevskoy and Bezymianny volcanoes (for details see [*Kiryukhin et al.*, 2023a; *Ozerov et al.*, 2020]) (left) and photos of the eruption of Klyuchevskoy volcano August 4–14, 2025 (photo by Yu. V. Demyanchuk). The section shows the projections of magmatic injections (dykes, sills) identified by seismic data from the local network of the KB GS RAS in 2025, with thick red lines, and magmatic injections (dykes, sills) after the $M_W = 8.8$ earthquake on July 29, 2025, with yellow lines. The circles represent the hypocenters of earthquakes (2000–2025) within ±2 km of the section plane. Notes: (1) Local earthquakes were not recorded between July 23 and August 13, 2025 due to regional aftershock interference; (2) axis markings in meters.

2.3.3. Krasheninnikov Volcano

For more than 600 years, this volcano was considered extinct. After the $M_W = 8.8$ earthquake on July 29, 2025, the Krasheninnikov volcano erupted on August 3, 2025 [*Gorbach et al.*, 2026; *Melnikov et al.*, 2026]. An eruption of the Krasheninnikov volcano began at 16:50 UTC on August 2, 2025, with ash explosions reaching up to 3–4 km above sea level. This is the first historic eruption of this volcano. According to satellite data by KVERT, explosions sent ash up to 8–8.5 km above sea level, and an ash plume is moving for 185 km to the east of the volcano, subsequently effusive activity of Krasheninnikov volcano began. It can be assumed that seismogenic fault #11 (Figure 12) played an important role in initiating the eruption of the Krasheninnikov volcano, providing an influx of water from the slab into the mantle wedge at the level of primary magma melting in the volcano's epicenter.

2.3.4. Karymsky Volcano

After the $M_W = 8.8$ earthquake on July 29, 2025, a series of seismic events were recorded on the Karymsky volcano on certain days, possibly accompanied by ash emissions up to 3,500 meters above sea level. "Volcano activity on Karymsky has resumed. Explosions sent ash up to 2 km above sea level, and an ash cloud 12×12 km in size is observed 26 km to the southeast of the volcano" (according to KVERT, dated August 14, 2025). It should be noted that since 1996, when a powerful $M_W = 7.2$ earthquake occurred near the volcano (60 km away) (Figure 1), the Karymsky volcano has been in a state of almost continuous steam-gas activity (sometimes cyclical with an interval of 10–15 minutes, like a geyser) with discrete steam-gas eruptions. This may indicate a significant role of water influx from the Karymsky Lake in the functioning of the Karymsky volcano's magmatic system.

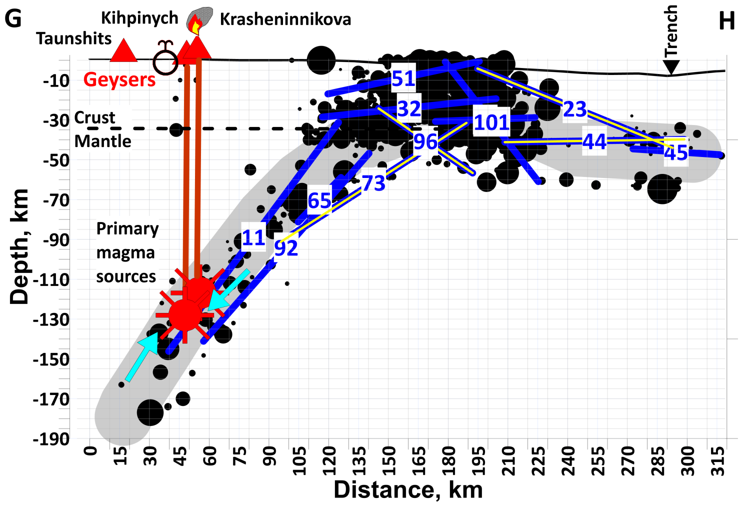

Figure 12. Transverse seismic-tectonic section of the Kamchatka subduction zone along the GH line (see Figure 1). Legend: blue numbered segments show traces of seismogenic faults (numbered according to Figure 1) on the plane of the section, seismogenic faults with the greatest aftershock activity (M_W = 8.8 July 29, 2025) are highlighted by thin yellow lines from the inside; black circles show projections of hypocenters earthquakes (1980–2025) recorded at a distance of 15 km from the incision plane, the size of the circles is proportional to the magnitude of the earthquakes; the area shaded in gray corresponds to the generalized position of the slab; the blue arrows show the expected discharge of water from the slab in the direction of the mantle wedge; the red circle with radial rays corresponds to the area of primary magma sources; the thick red line shows the direction of magma transport to the Earth's surface; active volcanoes are depicted with red triangles; the dotted line shows the assumed boundary of the crust and upper mantle.

It can be assumed that seismogenic fault #40 (Figure 13) played an important role in the restart of the Karymsky volcano eruption in August 2025, providing an influx of water from the slab into the mantle wedge at the level of primary magma melting in the volcano's epicenter.

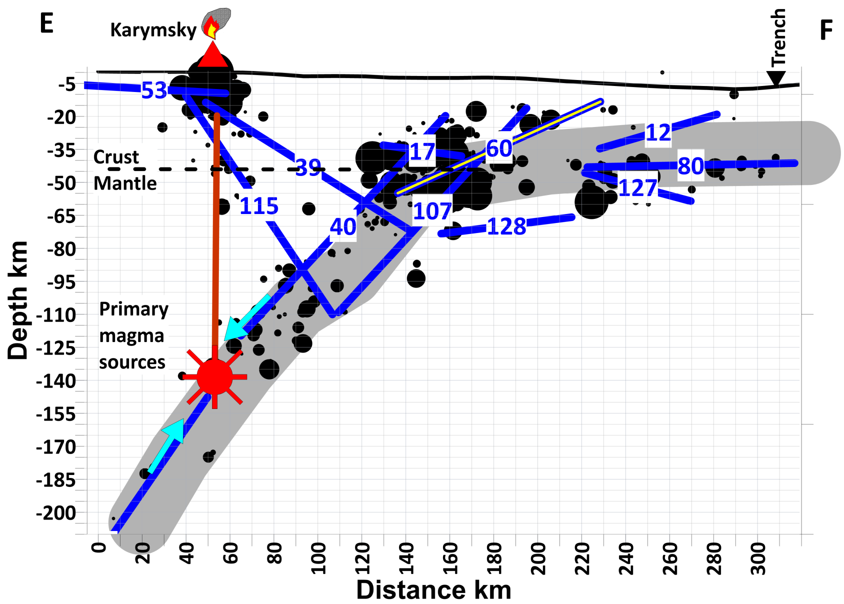

Figure 13. Transverse seismotectonic section of the Kamchatka subduction zone along the EF line (see Figure 1 for the section position). Legend: see Figure 12.

2.3.5. Avachinsky Volcano

A detailed description of the historical activity of the Avachinsky volcano and the latest data on fumarole emissions in the crater were provided in [*Malik*, 2024; *Melekestsev et al.*, 1994]. After the $M_W = 8.8$ earthquake on July 29, 2025, a glow was observed over the crater, and steam and gas emissions with a small amount of ash rose to a height of 300 m.

2.3.6. Kambalny Volcano

After the $M_W = 8.8$ earthquake on July 29, 2025, increased seismic activity was recorded in the volcano area, with up to 400 events per day. Of these, 20 events had K_s values ranging from 7 to 11.

3. Results and Discussion

The mechanisms of the strongest $M_W = 8.8$ earthquake on July 29, 2025 are characterized by (NEIC) two nodal planes NP1 (strike azimuth 198°, dip angle 18°, rake 51° (thrust-shear)) and NP2 (strike azimuth 58°, dip angle 76°, rake 101° (thrust)) (Table 1), with the compression/extending regions shown in Figure 14. Similar estimates of the mechanism are also presented in [*Xu et al.*, 2025] (Table 2).

Table 1. Earthquake mechanism on $M_W = 8.8$ July 29, 2025 from NEIC (52.498°N 160.264°E 35.0 km depth). T compression axis (plunge 58°, azimuth 344°)

Nodal planes	Strike	Dip	Rake	Dip Azimuth
NP1	198°	18°	51°	288°
NP2	58°	76°	101°	148°

Table 2. Earthquake mechanism on $M_W = 8.8$ July 29, 2025 from [*Xu et al.*, 2025]

Nodal planes	Strike	Dip	Rake	Dip Azimuth
NP1	212.6°	19.8°	81.2°	302.6°
NP2	41.9°	70.4°	98.8°	131.9°

For Kamchatka hydrogeological reservoirs, this mechanisms means a discrete increase in the fractured-pore space (in general) after the earthquake, and, as a result, a decrease in the pressure in the hydrogeological reservoirs. This is manifested by a decrease in the water level in the observation wells (piezometric level), a decrease in the flow rate of wells operating in the self-flow/pumping or complete shutdown of their operation.

These effects were recorded for the Vilyuchinsky, Paratunsky and Ketkinsky geothermal fields (cessation of self-discharge of well R27 and lowering of the water level by 4.5 m (Figure 5, Vilyuchinsky); decrease in flowrate of well K6 by 13% and a decrease in wellhead pressure by 0.4 bar at well K01 (Ketkinsky), a decrease in self-discharge rate at well GK1 (Ketkinsky, Figure 4); the cessation of self-discharge of the well K8 in the Yuzhno-Berezhny Site, reduction of parameters of the well 63 in the Northern Site and T3 of the Sredny site of the Paratunsky geothermal field. A discrete decrease in pressure in the Ketkinsky production reservoir by $\Delta P = 0.4$ bar (well K01, depth 2.3 km) with a porosity $\phi = 0.05$ and a pore compressibility $C = 7 \times 10^{-10}$ Pa^{-1} [*Kiryukhin et al.*, 2022a] corresponds to a volumetric co-seismic volumetric strain expansion $\varepsilon_V = 1.4 \times 10^{-6}$:

$$\varepsilon_V \approx \Delta\phi = \phi \cdot C \cdot \Delta P,$$

where pore compressibility C is given by [*Pruess et al.*, 1999]:

$$C = \frac{\Delta\phi}{\phi \cdot \Delta P}.$$

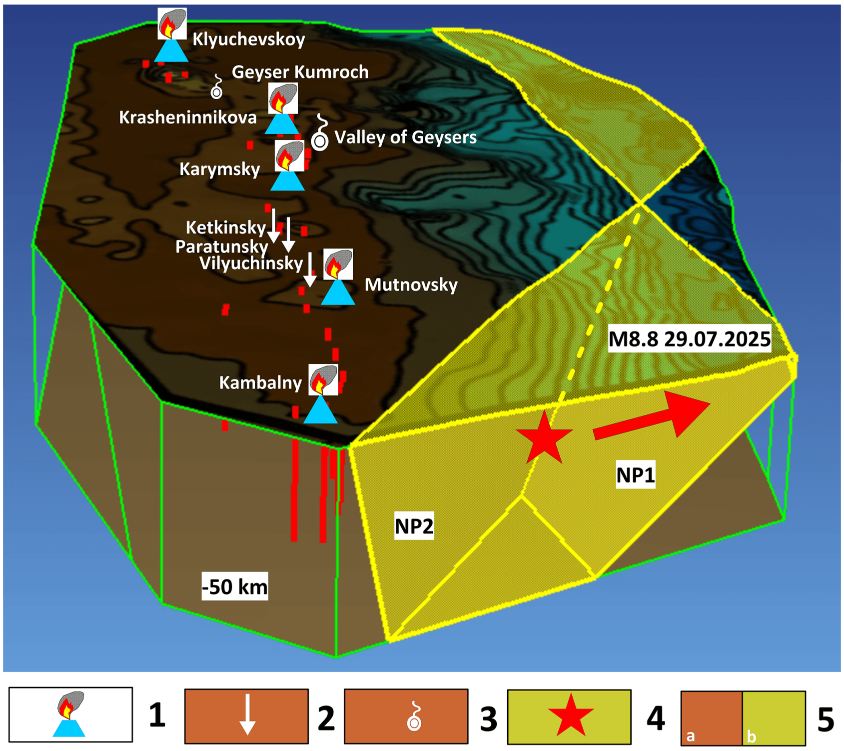

Figure 14. Geofluid systems of Kamchatka response to the strongest earthquake M_W = 8.8 on July 29, 2025. Legend: 1 – volcanoes that became active after the earthquake; 2 – hydrothermal reservoirs with observed discrete level drop and decreases the flow rate of wells; 3 – geysers; 4 – the hypocenter of the M_W = 8.8 earthquake; 5 – extension zone (a) and compression zone (b), according to the definition of the focal earthquake mechanism (NEIC). The red arrow shows the direction of movement of the hanging block along the nodal plane NP1 (left-hand thrust). The vertical and horizontal scale ratios are 2:1.

Another factor affecting the regional extending of hydrogeological reservoirs is the opening of cracks, including cracks in the caprock of thermal water reservoir, which isolates them from the influx of cold groundwater. This is especially important for the functioning of geysers, as the influx of cold water condenses the vapor-gas phase required for their gas lift eruptions mechanism [*Kiryukhin et al.*, 2022c, 2023b]. Monitoring data on the interval between eruptions of four geysers in the Valley of Geysers and the Uzon Caldera show that two geysers may have been affected: the Bolshoy geyser had at least 12 missed eruptions between May and August 2025, and the Grot geyser stopped functioning between February and March 2025 (Figure 7).

On the other hand, the opening of cracks in the hydrogeological reservoir itself can lead to the boiling of the carbon dioxide-saturated liquid phase and its transition to a geyser-like mode. The example of the Kumroch geyser-well shows this (see photo in Figure 8).

The effect of regional extension on the magmatic systems of volcanoes also leads to an increase in the volume of the latter and a decrease in the pressure of the liquid magmatic phase. When the pressure drops below the saturation pressure of the dissolved gases, the process of boiling begins, with increased vapor-gas activity and the potential for subsequent gas-lift eruptions. This is particularly critical for giant volcanoes like Klyuchevskoy (4850 m), where magma can reach the summit using gas only [*Eichelberger et al.*, 2020; *Eichelberger*, 2023].

Another factor associated with regional stretching is the reduction of horizontal stress [*Zoback*, 2010], which also creates favorable conditions for vertical fracturing and dyke formation.

Both of these factors probably worked in favor of the intensification of the eruption of the Klyuchevskoy volcano on August 8–12, 2025, when the greatest magmatic activity manifested in the shallow magmatic system of in the form of sills at about +1 km (see Figure 11). Regional seismotectonic crosssections through the Krasheninnikov and Karymsky volcanoes (Figures 12 and 13) show the absence of seismic activity of the slab under the volcanoes after the $M_W = 8.8$ earthquake (seismogenic faults with the greatest aftershock activity ($M_W = 8.8$ July 29, 2025) are highlighted by thin yellow lines from the inside in those Figures), i.e. these volcanoes operated in the mode of shallow magmatic activity. A local seismotectonic section through the Mutnovsky volcano (Figure 9) also shows shallow magmatic activity (above −2.5 km).

The area of the most significant impact of the earthquake on seismogenic faults covers an area of 400 km × 250 km up to a depth of 90 km (Figures 1, 12 and 13, the seismogenic faults with the greatest aftershock activity are highlighted by thin yellow lines from the inside). The population of the most active aftershock faults has a predominant north-west dip azimuth and is characterized by dip angles of 20–30° and 40–50° (Figure 2, right stereogram). This orientation and the orientation of the slab correspond to the nodal plane NP1 (strike azimuth 198° north-northeast, dip angle 18°, left-handed thrust-slip) of the $M_W = 8.8$ earthquake mechanism.

The conditions of horizontal extension in the south-east direction are detected by satellite geodetic data from GNSS (Global Navigation Satellite System) and InSAR (Interferometric Synthetic Aperture Radar) [*Mikhailov et al.*, 2025]. In the above-mentioned work, the maximum displacement along the satellite observation line is 130 cm in the south of Kamchatka, while the horizontal displacement is up to (151 cm E, −124 cm N) according to GNSS. An indirect sign of horizontal stretching is also the information posted on the website https://www.itpz-ran.ru/ru/model-ochaga-kamchatka-ru/ according to processed actual GNSS data, where Kamchatka (the eastern coast) sinks by 1 m or more.

The response of geofluid systems (volcanoes and geysers) to the strongest earthquakes is not random, as shown in the review [*Manga and Brodsky*, 2006], 0.4% of volcanic eruptions occur a few days after the remote strongest earthquakes, which is much higher than the average eruptive activity of volcanoes. At the same time, the authors suggest that boiling (formation of gas bubbles) in magmatic systems can be a trigger for eruptions, and the nucleation of gas bubbles is caused by the passage of seismic waves.

In the case of the $M_W = 8.8$ earthquake on July 29, 2025, the cause of the magmatic systems boiling could also be the regional stretching of the upper part of the Earth's crust, which is recorded by hydrogeological and satellite geodetic observations.

It is also necessary to further study the question of why, given the general geological trend of right-lateral shear at the Kamchatka-Slab boundary [*Kozhurin*, 2022; *Kozhurin and Zelenin*, 2017] and the expected sinking of the slab, the most likely mechanism of the $M_W = 8.8$ earthquake on July 29, 2025 is described by a left-lateral thrust.

4. Conclusions

- The strongest earthquake $MW = 8.8$ on July 29, 2025 in Kamchatka was accompanied by regional stretching, subsequent significant deformations of water-bearing rocks in the upper part of the Earth's crust, with volumetric strain extension up to $n \times 10^{-6}$, and various responses of geofluid systems.
- Hydrothermal reservoirs lowered the pressure (up to 0.45 bar) and reduced the rates of the wells (due to the increase in the fracture-pore space of the water-bearing rocks).
- The Bolshoy geyser showed gaps in its eruptions, and the Grot geyser stopped erupting (probably due to the depressurization and the gas lift cessation by infiltration of cold water). A geyser-well appeared in Kumroch (the CO_2 reservoir boiled over due to the increase in the pore space).
- The Klyuchevskoy and Krasheninnikov volcanoes began to erupt, and the Karymsky, Mutnovsky, and Kambalny volcanoes increased activity (suggesting the boiling of shallow magmatic systems during regional stretching).

- Seismogenic faults with a north-north-east orientation, close to the nodal plane NP1 of the proposed $MW = 8.8$ earthquake mechanism on July 29, 2025 (according to NEIC) and slip vectors suggested by GNSS observations [*Mikhailov et al.*, 2025], have been most active.

Acknowledgments. The study was conducted under the FWME-2024-0007 project at the Institute of Volcanology and Seismology of the Far Eastern Branch of the Russian Academy of Sciences. The authors express their gratitude to O. V. Bergal-Kuvikas for discussing the results, to V. I. Shevtsova for conducting observations at well R27, and to A. P. Korchagina, G. N. Markevich and E. V. Chernykh for their technical support, the authors also thank A. A. Lyubin, Director of the "Renewable Energy" branch of Kamchatskenergo PJSC, and M. L. Bezotechestvo, Head of the Mutnovsky Geothermal Power Plants, N. A. Romanov, Lead Hydrogeologist, for supporting the field studies at the Mutnovsk geothermal field and providing data on pressure and temperature changes at the condenser of the M GeoPP. The data used in the work were obtained with large-scale research facilities "Seismic infrasound array for monitoring Arctic cryolitozone and continuous seismic monitoring of the Russian Federation, neighbouring territories and the world" (https://ckp-rf.ru/usu/507436/, http://www.gsras.ru/unu/).

References

Andrew R. E. B. and Gudmundsson A. Volcanoes as elastic inclusions: Their effects on the propagation of dykes, volcanic fissures, and volcanic zones in Iceland // Journal of Volcanology and Geothermal Research. — 2008. — Vol. 177, no. 4. — P. 1045–1054. — https://doi.org/10.1016/j.jvolgeores.2008.07.025

Avdeiko G. P. and Palueva A. A. Historic analysis of seismicity and seismic hazard of the Kamchatkan subduction zone // Vestnik KRAUNTs. Nauki o Zemle. — 2010. — Vol. 1, no. 15. — P. 69–89. — (In Russian).

Avdeiko G. P. and Palueva A. A. The Kamchatka subduction zone: Seismotectonic regionalization and geodynamics // Journal of Volcanology and Seismology. — 2011. — Vol. 5, no. 1. — P. 1–16. — https://doi.org/10.1134/s0742046311010027

Avdeiko G. P. and Palueva A. A. Earthquake swarms in the Kamchatka subduction zone and estimation of possible tsunami generation locations // Journal of Volcanology and Seismology. — 2012. — Vol. 6, no. 4. — P. 268–280. — https://doi.org/10.1134/S0742046312030025

Björnsson G., Flovenz O., Saemundsson K., et al. Pressure Changes in Icelandic Geothermal Reservoirs Associated with Two Large Earthquakes in June 2000 // Proceedings, Twenty-Sixth Workshop on Geothermal Reservoir Engineering, January 29-31, 2001. — California : University, 2001.

Boldina S. V., Kopylova G. N. and Kobzev V. A. Study of Seismic Effects on Changes in Groundwater Pressure: Equipment and Some Well Observation Results for the Kamchatka Peninsula // Geodynamics & Tectonophysics. — 2022. — Vol. 13, no. 2. — https://doi.org/10.5800/gt-2022-13-2-0594

Chebrov V. N., Droznin D. V., Kugaenko Y. A., et al. The system of detailed seismological observations in Kamchatka in 2011 // Journal of Volcanology and Seismology. — 2013. — Vol. 7, no. 1. — P. 16–36. — https://doi.org/10.1134/s0742046313010028

Eichelberger J., Kiryukhin A., Mollo S., et al. Exploring and Modeling the Magma-Hydrothermal Regime // Geosciences. — 2020. — Vol. 10, no. 6. — P. 234. — https://doi.org/10.3390/geosciences10060234

Eichelberger J. C. How Much Magma Reservoir Pressure is Required to Build a Mountain? // Proceedings of All-Russian Scientific Conference with International Participation «Geothermal Volcanology, Hydrogeology, Oil and Gas Geology» (Geothermal Volcanology Workshop 2023). — Petropavlovsk-Kamchatsky : Institute of Volcanology, Seismology FEB RAS, 2023. — P. 65–70.

Fedotov S. A. Long-Term Seismic Forecast for the Kuril-Kamchatka Arc. — Moscow : Nauka, 2005. — 302 p. — (In Russian).

Fedotov S. A. Magmatic Feeding Systems and the Mechanism of Volcanic Eruptions. — Moscow : Nauka, 2006. — 456 p. — (In Russian).

Gorbach N. V., Ozerov A. Yu., Rogozin A. N., et al. First Historical Eruption of Krasheninnikov Volcano (Eastern Kamchatka): Field Observations and Composition of Lavas Erupted in August-September 2025 // Journal of Volcanology and Seismology. — 2026. — Vol. 20, no. 1. — P. 1–14. — https://doi.org/10.1134/S0742046325700678

Gordeev E. I., Koulakov I. Y. and Shapiro N. M. Peculiarities of Subduction in the Junction of the Kuril-Kamchatka and Aleutian Island Arcs // Doklady Earth Sciences. — 2020a. — Vol. 494, no. 2. — P. 790–794. — https://doi.org/10.1134/s1028334x20100050

Gordeev E. I., Koulakov I. Y. and Shapiro N. M. The Magma Feeding System of the Klyuchevskaya Group of Volcanoes (Kamchatka) // Doklady Earth Sciences. — 2020b. — Vol. 493, no. 2. — P. 627–631. — https://doi.org/10.1134/s1028334x20080085

Gudmundsson A. How local stresses control magma-chamber ruptures, dyke injections, and eruptions in composite volcanoes // Earth-Science Reviews. — 2006. — Vol. 79, no. 1/2. — P. 1–31. — https://doi.org/10.1016/j.earscirev.2006.06.006

Gudmundsson A. Deflection of dykes into sills at discontinuities and magma-chamber formation // Tectonophysics. — 2011. — Vol. 500, no. 1–4. — P. 50–64. — https://doi.org/10.1016/j.tecto.2009.10.015

Gudmundsson A. Introduction // Volcanotectonics: Understanding the Structure, Deformation and Dynamics of Volcanoes. — Cambridge University Press, 2020. — P. 1–33. — https://doi.org/10.1017/9781139176217.002

Gudmundsson A. The propagation paths of fluid-driven fractures in layered and faulted rocks // Geological Magazine. — 2022. — Vol. 159, no. 11/12. — P. 1978–2001. — https://doi.org/10.1017/s0016756822000826

Gudmundsson A. and Andrew R. E. B. Mechanical interaction between active volcanoes in Iceland // Geophysical Research Letters. — 2007. — Vol. 34, no. 10. — https://doi.org/10.1029/2007GL029873

Kiryukhin A. Modeling and observations of geyser activity in relation to catastrophic landslides-mudflows (Kronotsky nature reserve, Kamchatka, Russia) // Journal of Volcanology and Geothermal Research. — 2016. — Vol. 323. — P. 129–147. — https://doi.org/10.1016/j.jvolgeores.2016.05.008

Kiryukhin A. V., Bergal-Kuvikas O. V. and Lemzikov M. V. Magmatic activity of Klyuchevskoy volcano triggering eruptions of Bezymianny volcano based on seismological and petrological data // Journal of Volcanology and Geothermal Research. — 2023a. — Vol. 442. — P. 107892. — https://doi.org/10.1016/j.jvolgeores.2023.107892

Kiryukhin A. V., Fedotov S. A. and Kiryukhin P. A. A geomechanical interpretation of the local seismicity related to eruptions and renewed activity on Tolbachik, Koryakskii, and Avacha Volcanoes, Kamchatka, in 2008-2012 // Journal of Volcanology and Seismology. — 2016. — Vol. 10, no. 5. — P. 275–291. — https://doi.org/10.1134/S0742046316040047

Kiryukhin A. V., Nazhalova I. N. and Zhuravlev N. B. Hot water-methane reservoirs at southwest foothills of Koryaksky volcano, Kamchatka // Geothermics. — 2022a. — Vol. 106. — P. 102552. — https://doi.org/10.1016/j.geothermics.2022.102552

Kiryukhin A. V., Polyakov A. Y., Voronin P. O., et al. Magma fracking and production reservoirs beneath and adjacent to Mutnovsky volcano based on seismic data and hydrothermal activity // Geothermics. — 2022b. — Vol. 105. — P. 102474. — https://doi.org/10.1016/j.geothermics.2022.102474

Kiryukhin A. V., Polyakov A. Y., Zhuravlev N. B., et al. Dynamics of natural discharge of the hydrothermal system and geyser eruption regime in the Valley of Geysers, Kamchatka // Applied Geochemistry. — 2022c. — Vol. 136. — P. 105166. — https://doi.org/10.1016/j.apgeochem.2021.105166

Kiryukhin A. V., Sergeeva A. V. and Usacheva O. O. Modeling of the thermal-hydrodynamic and chemical regime of Geyser reservoir (Valley of Geyser, Kamchatka) // Geothermics. — 2023b. — Vol. 115. — P. 102808. — https://doi.org/10.1016/j.geothermics.2023.102808

Kiryukhin A. V., Sergeeva A. V., Usacheva O. O., et al. Thermal-Hydrodynamic Modeling of the Valley of Geysers and Kikhpinych Volcano Magma-Hydrothermal System // JP Journal of Heat and Mass Transfer. — 2025. — Vol. 38, no. 1. — P. 127–168. — https://doi.org/10.17654/0973576325007

Kiryukhin A. V., Vorozheikina L. A., Voronin P. O., et al. Thermal and permeability structure and recharge conditions of the low temperature Paratunsky geothermal reservoirs in Kamchatka, Russia // Geothermics. — 2017. — Vol. 70. — P. 47–61. — https://doi.org/10.1016/j.geothermics.2017.06.002

Kiryukhin A. V. and Yampolsky V. A. Modeling study of the Pauzhetsky geothermal field, Kamchatka, Russia // Geothermics. — 2004. — Vol. 33, no. 4. — P. 421–442. — https://doi.org/10.1016/j.geothermics.2003.09.010

Kissin I. G. Fluids in the Earth's Crust. Geophysical and Tectonic Aspects. — Moscow : Nauka, 2009. — 328 p. — (In Russian).

Kopylova G. and Boldina S. Seismo-Hydrogeodynamic Effects in Groundwater Pressure Changes: A Case Study of the YuZ-5 Well on the Kamchatka Peninsula // Water. — 2023. — Vol. 15, no. 12. — P. 2174. — https://doi.org/10.3390/w15122174

Kopylova G. and Boldina S. A Verification of Seismo-Hydrogeodynamic Effect Typifications Recorded in Wells on the Kamchatka Peninsula: The 3 April 2023 Earthquake, Mw = 6.6, as an Example // Water. — 2025. — Vol. 17, no. 5. — P. 634. — https://doi.org/10.3390/w17050634
Kozhurin A. Active faults in Sakhalin and North of the Sea of Okhotsk: Does the Okhotsk plate really exist? // Journal of Asian Earth Sciences. — 2022. — Vol. 230. — P. 105219. — https://doi.org/10.1016/j.jseaes.2022.105219
Kozhurin A. and Zelenin E. An extending island arc: The case of Kamchatka // Tectonophysics. — 2017. — Vol. 706/707. — P. 91–102. — https://doi.org/10.1016/j.tecto.2017.04.001
Lobkovsky L. I. and Baranov B. V. A key model of strong earthquakes in island arcs and active continental margin of zones // Doklady Akademii Nauk SSSR. — 1984. — Vol. 275, no. 4. — P. 843–847. — (In Russian).
Malik N. A. A decade (2013-2023) of direct sampling from high-temperature fumaroles at Avacha Volcano, Kamchatka: Gas geochemistry, seasonal and long-term variations // Journal of Volcanology and Geothermal Research. — 2024. — Vol. 455. — P. 108179. — https://doi.org/10.1016/j.jvolgeores.2024.108179
Manga M. and Brodsky E. Seismic Triggering of Eruptions in the Far Field: Volcanoes and Geysers // Annual Review of Earth and Planetary Sciences. — 2006. — Vol. 34, no. 1. — P. 263–291. — https://doi.org/10.1146/annurev.earth.34.031405.125125
McClure M. W. Modeling and characterization of hydraulic stimulation and induced seismicity in geothermal and shale gas reservoirs : PhD thesis / McClure M. W. — USA, 2012.
Melekestsev I. V., Braitseva O. A., Dvigalo V. N., et al. Historical eruptions of the Avacha volcano in Kamchatka (an attempt of modern interpretation and classification for long-term prediction of the type and parameters of future eruptions). Part II (1926-1991) // Volcanology & Seismology. — 1994. — Vol. 16, no. 2. — P. 93–114.
Melnikov D. V., Ozerov A. Yu. and Bakhmatova Y. A. Application of VIIRS Nightfire data for monitoring the current eruption of Krasheninnikov volcano (Kamchatka): first results and possible connection with a strong earthquake // Volcanism and related processes. Proceedings of the XXIX annual scientific conference dedicated to the Volcanologist Day, March 30 - April 4, 2026. — Petropavlovsk-Kamchatsky : IVS FEB RAS, 2026. — P. 100–103. — (In Russian).
Mikhailov V. O., Konvisar A. M., Smirnov V. B., et al. The Rupture Surface Model of the July 29, 2025 Mw 8.8 Kamchatka Earthquake Based on Satellite Geodesy and Interferometry Data // Doklady Earth Sciences. — 2025. — Vol. 525, no. 2. — https://doi.org/10.1134/s1028334x25608752
Ozerov A. Yu., Girina O. A., Zharinov N. A., et al. Eruptions in the Northern Group of Volcanoes, in Kamchatka, during the Early 21st Century // Journal of Volcanology and Seismology. — 2020. — Vol. 14, no. 1. — P. 1–17. — https://doi.org/10.1134/S0742046320010054
Pruess K., Oldenburg C. and Moridis G. TOUGH2 User's Guide Version 2. — California : Office of Scientific, Technical Information (OSTI), 1999. — https://doi.org/10.2172/751729
Seliverstov N. I. Structure of Kamchatka seismo-focal zone // Vestnik KRAUNTs. Nauki o Zemle. — 2007. — Vol. 1. — P. 10–26. — (In Russian).
Sigmundsson F., Hooper A., Hreinsdóttir S., et al. Segmented lateral dyke growth in a rifting event at Bárḥarbunga volcanic system, Iceland // Nature. — 2015. — Vol. 517, no. 7533. — P. 191–195. — https://doi.org/10.1038/nature14111
Xu D., Wang W. and Ren Z. Preliminary slip distribution of the July 29, 2025 M 8.8 Kamchatka, Russia earthquake // Earthquake Research Advances. — 2025. — P. 100427. — https://doi.org/10.1016/j.eqrea.2025.100427
Zavaritsky A. N. Volcanoes of Kamchatka. — Moscow : AN SSSR, Trudy Laboratorii Vulkanologii. Vypusk 10, 1955. — (In Russian).
Zelenin E., Bachmanov D., Garipova S., et al. The Active Faults of Eurasia Database (AFEAD): the ontology and design behind the continental-scale dataset // Earth System Science Data. — 2022. — Vol. 14, no. 10. — P. 4489–4503. — https://doi.org/10.5194/essd-14-4489-2022
Zoback M. D. Reservoir Geomechanics. — Cambridge University Press, 2010. — 449 p.